



Nuclear Materials Authority
P.O.Box 530 Maadi, Cairo, Egypt

DOAJ DIRECTORY OF
OPEN ACCESS
JOURNALS

ISSN 2314-5609
Nuclear Sciences Scientific Journal
13, 1- 26
2024
<https://nssi.journals.ekb.eg>

AURIFEROUS QUARTZ VEINS AT ROMIT AREA, SOUTH EASTERN DESERT, EGYPT: GEOLOGIC SETTING AND GEOCHEMICAL SIG- NATURE

MOSTAFA M. BAYOUMI and DOAA A. MOSTAFA

Nuclear Materials Authority, P.O. Box 530 Maadi, Cairo, Egypt

ABSTRACT

Romit area is located in the southern part of Eastern Desert and covered by late Proterozoic igneous and metamorphic rocks. Metavolcanics and tonalite-granodiorites form most of the main outcrops in the area, which is cut off by quartz veins carrying radioactive and rare earth elements, in addition to gold. Major oxides were analyzed using conventional wet chemical analysis, trace element using X-ray fluorescence (XRF), rare earth elements (REE's) by an Inductively Coupled Plasma Emission Spectrometry (ICP-ES) and U and Th chemically by Arsenazo III. The heavy minerals were investigated by using environmental scanning electron microscope (ESEM) and identified by X-ray diffraction technique (XRD). Gold concentration was confirmed using fire assay methods (EMRA). This work aims to study the geologic, geochemical and mineralogical characteristics of auriferous uraniumiferous quartz veins at the Romit area. The discovery of radionuclides and gold mineralization were recorded in quartz veins for the first time. The Romit quartz veins have relatively high uranium and thorium contents. The average uranium and thorium contents are 49 ppm and 75 ppm, respectively. The quartz veins of the Romit area show enrichment in some rare metal (Zr, Y, Nb, Pb and Au). The high content in some rare metal in these quartz veins is due to the invading hydrothermal fluids in the later stages of magmatic activity. So, these hydrothermal fluids are potentially important in the dissolution, transportation and precipitation of these elements in these quartz veins. Generally, the rock is characterized by relatively high content of rare earth elements and characterized by negative Eu and Ce anomalies. The identified minerals in the studied quartz veins can be grouped into U-Th-REE-bearing minerals (kasolite, uranothorite, columbite, monazite, allanite and xenotime), base metal minerals (gold, cerussite, pyrite and arsenopyrite), Oxide minerals (chromite, goethite, rutile and pyrolusite) and silicate minerals (kaolinite and spessartine). Environmental Scan Electron Microscope (ESEM) and fire assay techniques in quartz veins with high contents reach up to more than 1 ppm.

INTRODUCTION

Romit area lies at Gabal Ti Keferiai which is located at the extreme southern part of the Eastern Desert of Egypt in the Halaib district near the Sudan frontier between Lat. 22° 14' 29" and 22° 28' 25" N and Long. 35° 34' 21"

and 36° 01' 09" E. This area lies at a distance of about 65 km North West of Abu Ramad City. The study area is a part of metavolcanic belts along Wadi Ed Direra area (FigS. 1,2). Recently, there is no previous work about Romit area. The general geology of the Halaib district was studied by several authors (e.g.,

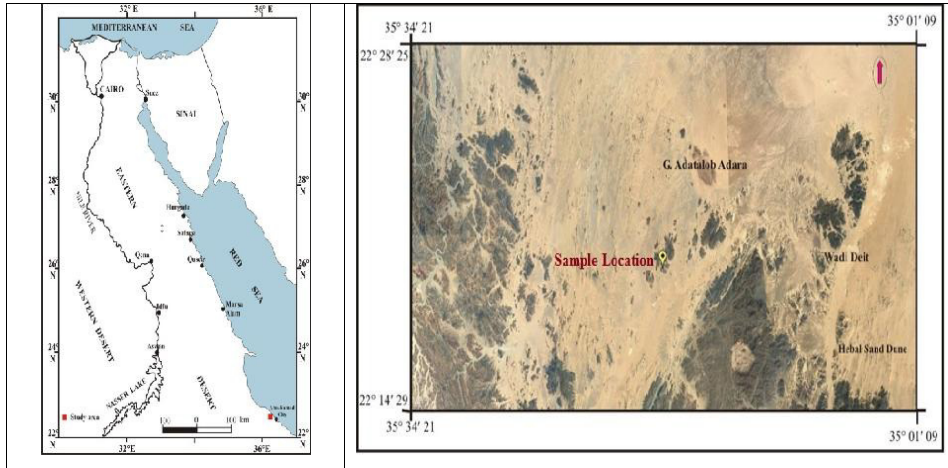


Fig. 1: Location map and Aerial photograph for Romit area Eastern Desert

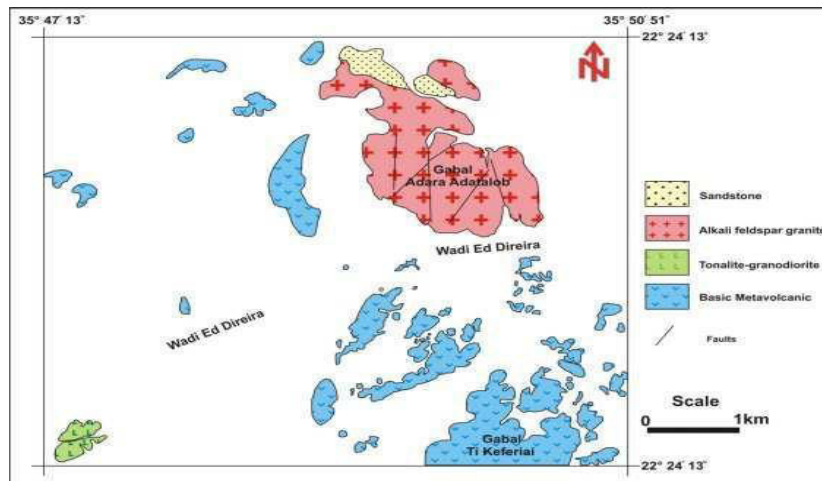


Fig. 2: Geologic Map of Gabal Adara Adatalob area, South Eastern Desert, Egypt (Shahin et al., 2014)

Hume, 1937; El-Ramly, 1972; Hussein, 1977; Kabesh, 1994; Assaf et al., 1998 and Ramadan, 2003). The mineral deposits of the district were also investigated by numerous authors (e.g., Bassiuny, 1957; El-Shazly and Saleeb 1959; Basta and Saleeb, 1971; Tak-

la et al., 1976; Hussein, 1990; Dardeir et al., 1992; El-Alfy et al., 1994; El Gammal and Cherif, 1999 and Ramadan, 2003). The radioactive mineralizations of the Egyptian Eastern Desert have been studied by many authors (e.g. El Ghawaby, 1973; El Shazly

and El Ghawaby, 1974; El Kassas, 1974; Ammar, 1997; Ramadan et al., 2004; Ammar et al., 2016 and Zeid, 2020).

Quartz is the most important silica mineral and widely occurs in igneous, metamorphic, sedimentary and hydrothermal rocks of the Earth's crust. Because of its abundance and properties, quartz finds many applications in industry and scientific researches (Götze, 2012). For instance, its luminescence, geochemical properties and hosting fluid/mineral inclusions have provided critical knowledge for reconstructing geological processes (Burley et al., 1989 and Rusk, 2012). In hydrothermal ore deposits, quartz is the most common gangue mineral and may intergrow with metals (such as native gold) and sulfides containing metals such as copper, tin, and tungsten (Pirajno, 2009).

The present work throws light on the geology, mineralogy of the area. It also, focuses on the new occurrence of gold mineralization and geochemistry of rare earth elements (REE) in the quartz veins of Romit area.

GEOLOGICAL SETTING

The rocks in the area are represented by the metavolcanic, tonalite granodiorite, alkali

feldspar granite and sandstone.

Moderate to high relief terrain, mainly covered by igneous and metamorphic rocks (Fig. 3), characterizes the study area. Metavolcanics and tonalite-granodiorites form most of the outcrops in the area. Metavolcanics are composed mainly of metarhyodacite and metarhyolite. They are fine grained, massive and vary in color from light gray and dark gray to pinkish gray. The weathered surfaces of metavolcanics range in color from greenish gray to pinkish dark gray. They show high luster and break with a conchoidal fracture (Fig. 4). These rocks are highly altered, weathered, exfoliated, and composed mainly of quartz, plagioclase, biotite and some muscovite (Fig. 5). Metavolcanics are fragmented and highly dissected by several trends of joints. They are fractured, jointed and characterized by porphyritic textures (Fig. 6). It is common to see hematitic and kaolinitic alterations, especially at fault intersections and along fractures. They are often injected along the extension planes. Field relations reveal that they are intruded by metamorphosed sandstone with sharp contact. This metamorphosed sandstone rock is fine-grained, pinkish white in color, highly sheared, highly jointed and banded. This metamorphosed sandstone is found forming a cap cover the top part in the northern side



Fig. 3: Photograph showing general view for Romit area



Fig. 4: Photograph showing conchoidal shape of metavolcanics



Fig. 5: Photograph showing fine-grained metavolcanics occurring as sheets

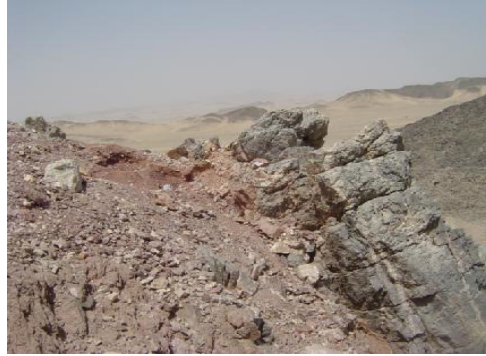


Fig. 7: Photograph showing basic dyke cut the metavolcanic



Fig. 6: Photograph showing jointing and fracturing of metavolcanic



Fig. 8. Photographs showing quartz veins

of the study area and the metavolcanic rocks form moderate to high relief of grey to dark grey and composed mainly of schistose chloritized metatuffs and meta- andesite.

Several types of dykes cut through the rock parts in the working area where, basic dykes are more abundant than acidic dykes (Fig. 7). All the dykes extend in a NW direction parallel to the trend of the shear zone. The acidic dykes are represented by a rhyodacite and occur in the northern part of the study area. The basic dykes are represented by andesite. The andesite is recorded all over the mine area. Quartz veins are also recorded cutting through all rock units (Fig. 8). The average content of

gold in the smoky quartz veins is higher than that of the milky quartz veins. This is probably due to the fact that record of the gold mineralization in the Eastern Desert is commonly associated with smoky quartz (Takla et al, 1995).

SAMPLING AND METHODOLOGY

Six samples were collected from the quartz veins of Romit area and subjected to mineralogical studies and chemical analyses. For the mineralogical investigations, heavy liquids separation technique was used to concentrate the heavy minerals. The heavy minerals were picked under binocular microscope and investigated by using environmental scanning elec-

tron microscope (ESEM) investigation. The EDAX analysis is considered as semi-quantitative analysis.

Determination of U and Th chemically was carried out by Arsenazo III using spectrophotometer model Prolabo, Jean and constant U.V. The major oxides are analyzed using conventional wet chemical techniques of Shapiro and Brannock (1962). Trace element concentrations were determined using an X-ray fluorescence (XRF) spectrometer from PHILIPS, model X'Unique-II. Rare earth elements (REE's) are measured using an Inductively Coupled Plasma Emission Spectrometry (ICP-ES). The Egyptian Nuclear Materials Authority's labs performed all the aforementioned tests (NMA).

For measuring gold concentrations, fire assay analyses were carried out at the Egyptian Mineral Resources Authority (EMRA), Central Laboratory Sector. Weigh 50 g of the sample, addition of flux (litharge – borax – sodium carbonate – flour – silica – silver), mixing the sample with flux in a ceramic crucible, melting of (sample + flux) at 1000° C for 1.5 hours, cupellation of (lead + gold +silver) alloy at 900°C for 1 hour, parting of resulting (gold – silver) alloy in nitric acid and aqua regia heating to get gold solution, and finally, analysis of gold solution by GBC Avanta atomic absorption instrument to get

gold concentration with ppm.

MINERALOGICAL STUDIES

The studied mineralization of Romit area can be classified into the following groups: (1) U-Th-REE-bearing minerals (2) Base metal minerals (3) Oxide minerals (4) Silicate minerals

U-Th-REE-Bearing Minerals

Kasolite [$\text{Pb}(\text{UO}_2)\text{SiO}_4 \cdot \text{H}_2\text{O}$] is generally distinguished from the other uranium silicates by its crystal habit and luster. It is present as yellow crystallites (Fig. 9) with resinous luster. The X-ray diffraction analysis detected the presence of kasolite mineral (Fig. 9). The EDAX analysis data refer to presence of 52.93% U, 39.29% Pb and 5.66% Si with traces of Fe and K (Fig. 10).

Uranothorite $(\text{Th,U})\text{SiO}_4$, has dark brown and brownish to pale-brownish colour (Fig. 11). The uranothorite was determined by X-ray diffraction (Fig. 11). From the EDX data, uranothorite contains an average 51.34% Th and 9.57% U (Fig. 12), it contains considerable amounts of Pb, Ca and Mn but it is almost free of any REE.

Columbite $[(\text{Fe,Mn,Mg})(\text{Nb,Ta})_2\text{O}_6]$, is black to dark brown tabular or rounded crystals (Fig. 13) with sub-metallic to resinous

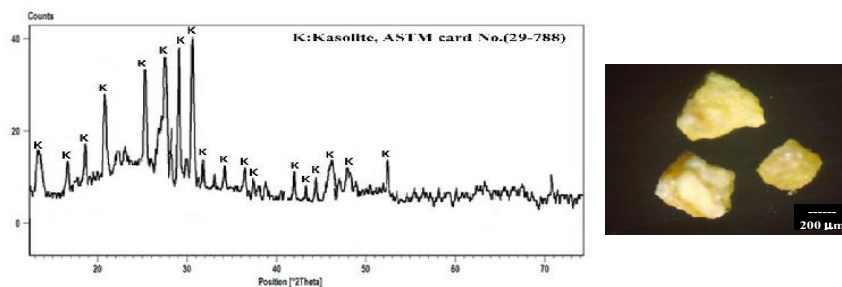


Fig. 9: X-ray diffraction patterns of kasolite

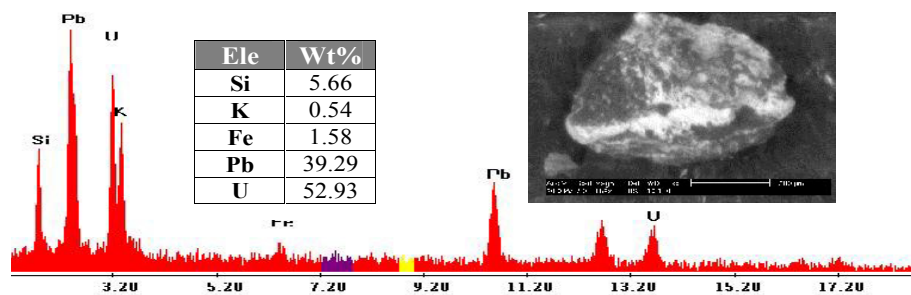


Fig.10: ESEM image and EDX analysis data of Kasolite

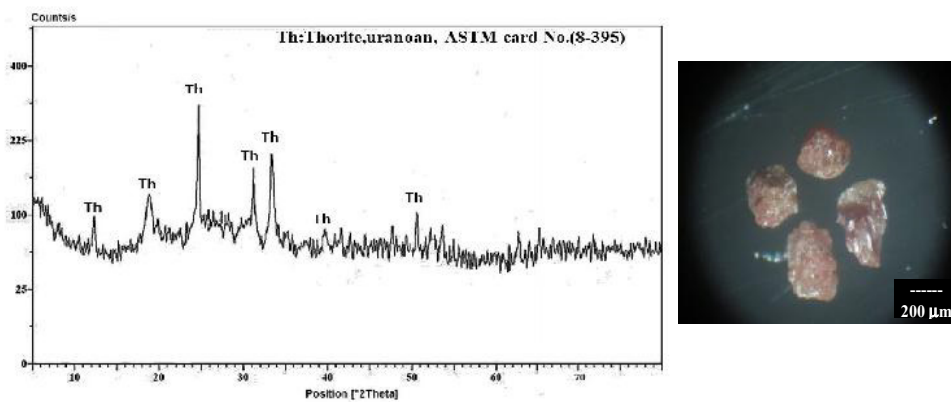


Fig. 11: X-ray diffraction patterns of uranothorite

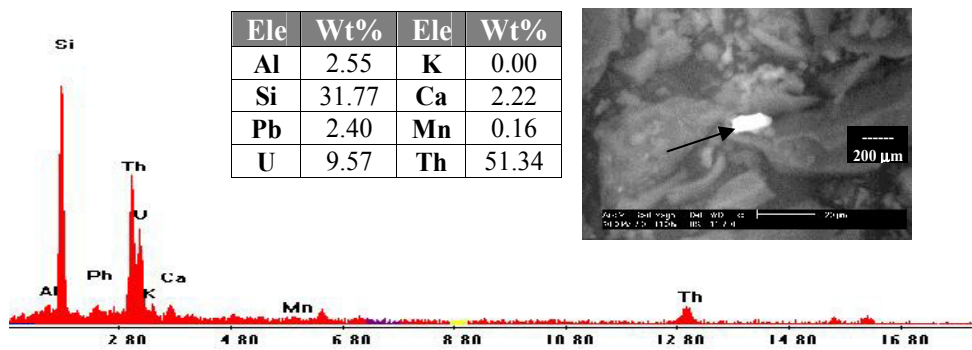


Fig.12: ESEM image and EDX analysis data of uranothorite

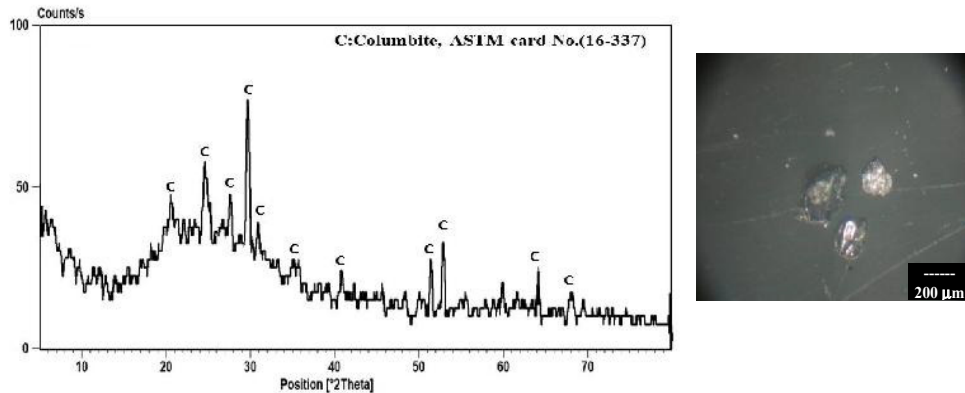


Fig.13: X-ray diffraction patterns of columbite

luster. The XRD analysis confirmed the identification of columbite mineral (Fig. 13). The EDX analyses show that columbite composed mainly of 42.49% Nb, 5.95% Ta and 2.15 U (Fig. 14).

Xenotime (YPO₄), exhibits translucent yellowish red to reddish brown colors (Fig. 15) with resinous luster. Besides Y, other rare earth elements (REE), predominantly heavy rare elements (HREE), and the actinide elements U and Th, are incorporated preferentially at the eight-fold lattice site in the xenotime-Y structure. It is easily recognized by XRD technique (Fig. 15). It is confirmed by

SEM-EDX technique and contains 30.67% Y and 6.93% P (Fig. 16).

Allanite [(Ce,Ca,Y,La) (Al,Fe⁺³)₃(SiO₄)₃.OH], is one of epidote group which can incorporate significant amounts of U, Th and LREE. The presence of the most radioactive elements in most cases led to breakdown of its crystal structure and allanite inverted into amorphous substance due to the radioactive emanations (Keer, 1959). From the EDX data allanite contains an average 35.09% Ce, 14.89% La, 10.13% Nd, 3.53% Pr, 1.47% Sm, 2.76% Gd and considerable amounts of Ca, Fe, Al, S and Si (Fig.17).

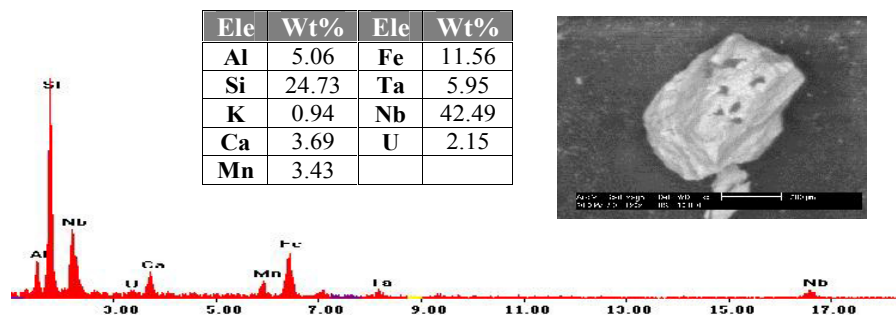


Fig.14: ESEM image and EDX analysis data of columbite

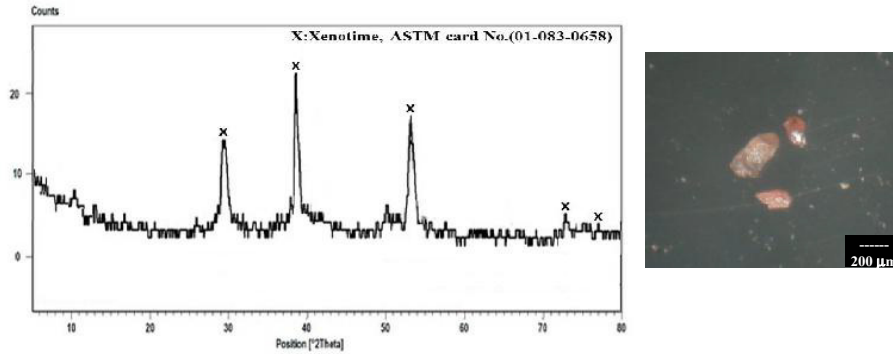


Fig.15: X-ray diffraction patterns of xenotime

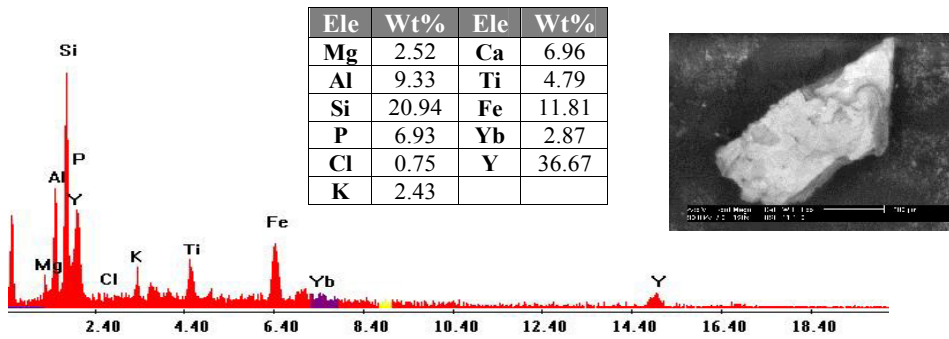


Fig.16: ESEM image and EDX analysis data of xenotime

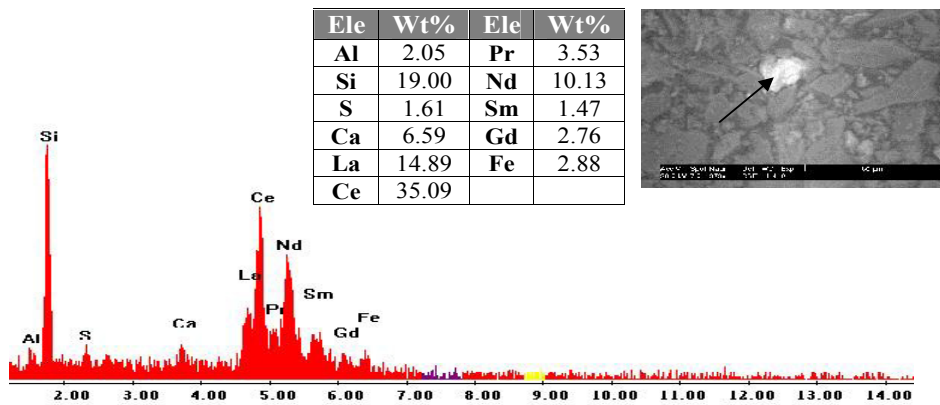


Fig.17: ESEM image and EDX analysis data of allanite

Monazite (Ce,La)PO₄ is a chief rare earth-bearing phosphate mineral occurring as accessory mineral. Monazite crystals occur as brown to reddish brown prismatic or tabular habit. Lazareva (2018) concluded that the monazite structure would accept REE ions radii between those of La and Eu. Based on the existence of a solid –solution series between (Ce, La) PO₄ and Ca Th (PO₄), the structure will accommodate ions with radii between those of Ce and Ca. EDX analysis revealed the presence of monazite (Fig. 18).

Base Metal Minerals

Gold (Au), it one of the rarest metals in the earth’s crust with an average grade of only 0.002 ppm Au. In comparison, silver average 0.08 parts per million (ppm) and platinum average 0.01 ppm (ppm) in the earth’s crust. Gold’s rarity and bright color have long attracted humans, and objects created from the precious metal have been documented as far back as 5,000 B.C. It is a yellow precious metal and analyzed by ESEM technique contains 68.29% Au in selected spot and found associated with As and Cl (Fig.19).

Pyrite (FeS), represent the most rich

and extensive sulphide mineral. It occurs in many hydrothermal vein deposits over a wide range in temperatures. Its color is yellowish gray to gray with metallic luster. It is identified by X-ray diffraction associated with arsenopyrite (Fig. 20). ESEM analysis shows that pyrite contains 43.55% Fe, 51.33% S (Fig.20).

Arsenopyrite (FeAsS), occurs as steel gray to silver white crystals (Fig.21). Large levels of gold may be found in association with arsenopyrite. As a result, it can be used as a marker for reefs that actually contain gold. Arsenopyrite occurs in hydrothermal veins and zones of contact metamorphism or metasomatism where temperatures are high. The X-ray diffraction analysis detected the presence of arsenopyrite mineral associated with pyrite (Fig. 21). The EDAX analysis data refer to presence of 34.55% Fe, 44.86% As and 20.59% S (Fig.22).

Cerussite (PbCO₃), is a mineral for lead and is a public alteration product of galena and occurs as yellowish color with sub-rounded form. EDAX analysis data show that cerussite have 88.11% Pb (Fig. 23).

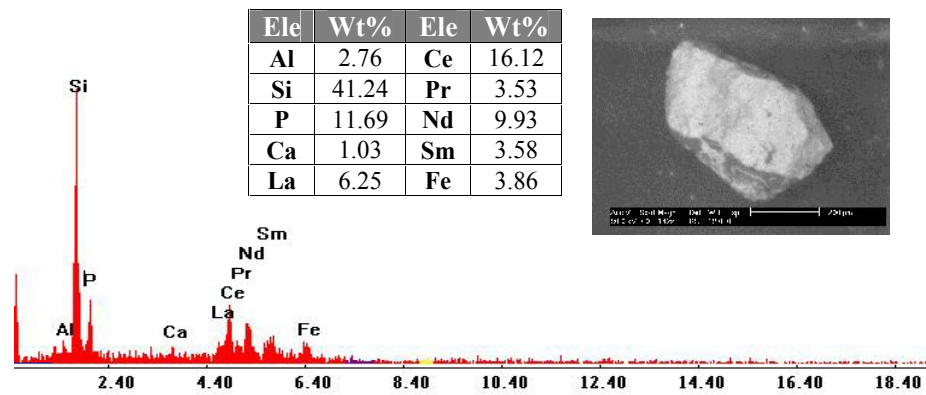


Fig.18: ESEM image and EDX analysis data of monazite

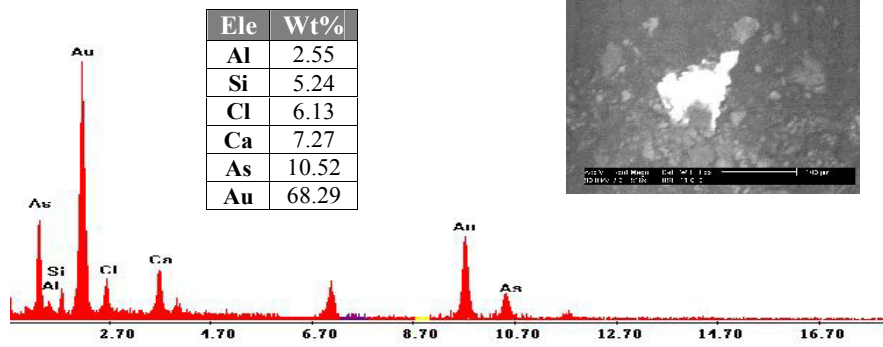


Fig.19: ESEM image and EDX analysis data of gold

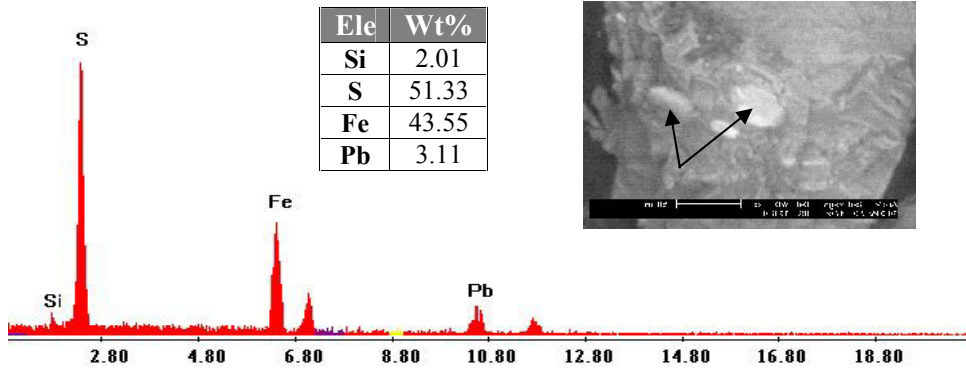


Fig.20: ESEM image and EDX analysis data of pyrite

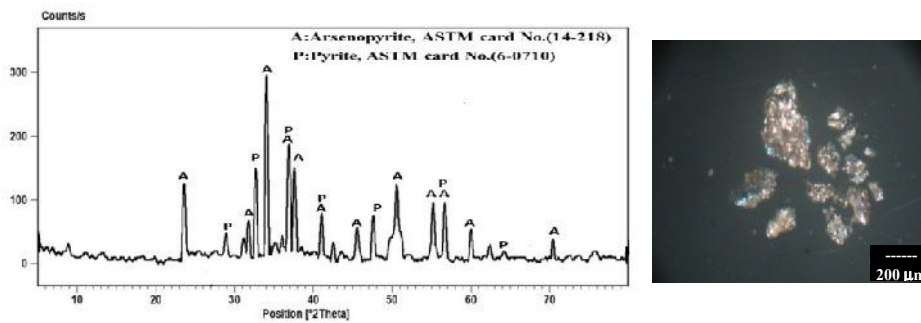


Fig.21: X-ray diffraction patterns of arsenopyrite

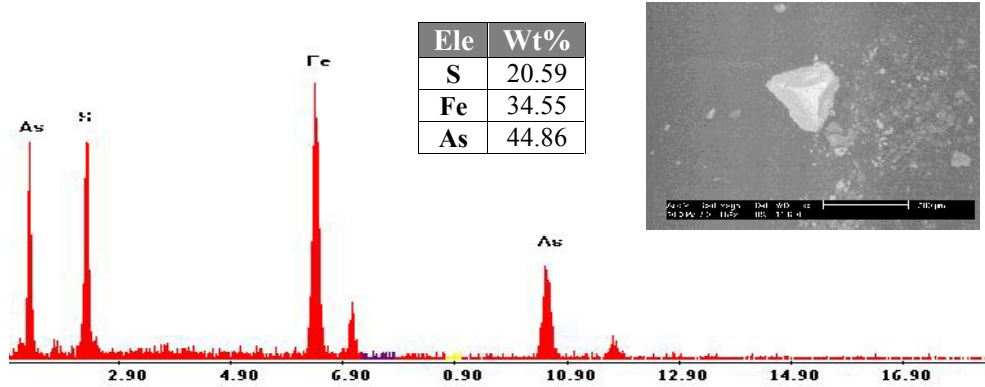


Fig.22: ESEM image and EDX analysis data of arsenopyrite

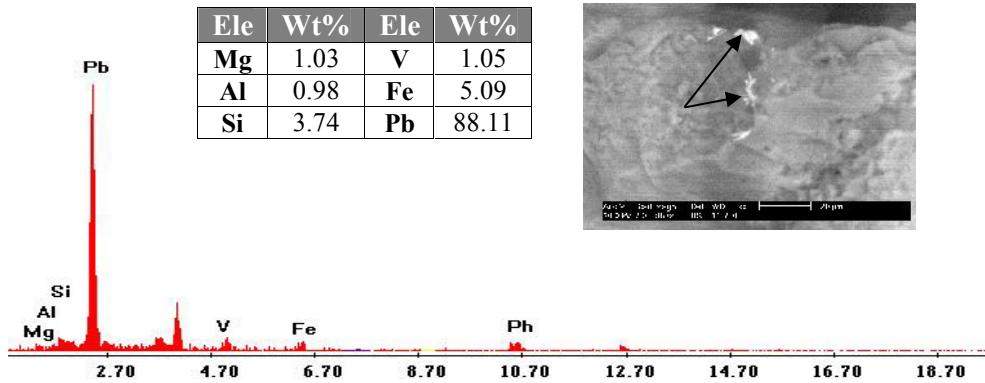


Fig.23: ESEM image and EDX analysis data of cerussite

Oxide Minerals

Chromite ($FeCr_2O_4$), is commonly located in the rocks in the studied area. Chromite appears as massive grains of black to brownish black color and has metallic luster. The SEM data of chromite shows its main constituents as 74.28% Fe and 10.86% Cr (Fig. 24).

Goethite ($FeO.OH$), is formed by the oxidation and hydration of iron minerals or as a direct precipitate. Goethite is produced as a

result the entirely oxidation of pyrite. Goethite is brilliant brown to black (Fig. 25) with brilliant black streak and sub- metallic to metallic luster. Goethite identified by XRD and EDX analysis (Fig. 25,26).

Rutile (TiO_2), is a major mineral source of the titanium, it typically includes about 60% titanium and 40% oxygen. It can have some iron, sometimes up to 10%. It is euhedral to subhedral elongated grains with brown red colour and rode-like crystal habit (Fig. 27). Ru-

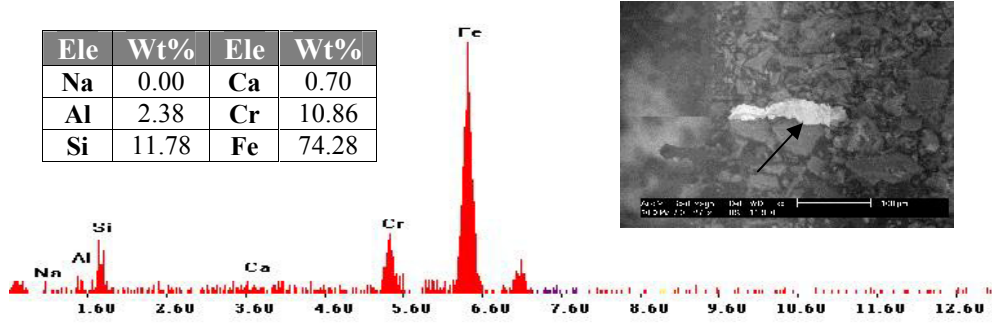


Fig.24: ESEM image and EDX analysis data of chromite

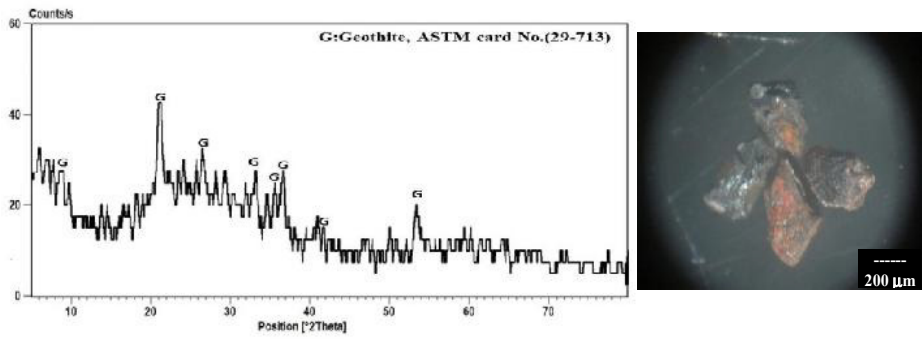


Fig.25: X-ray diffraction patterns of goethite

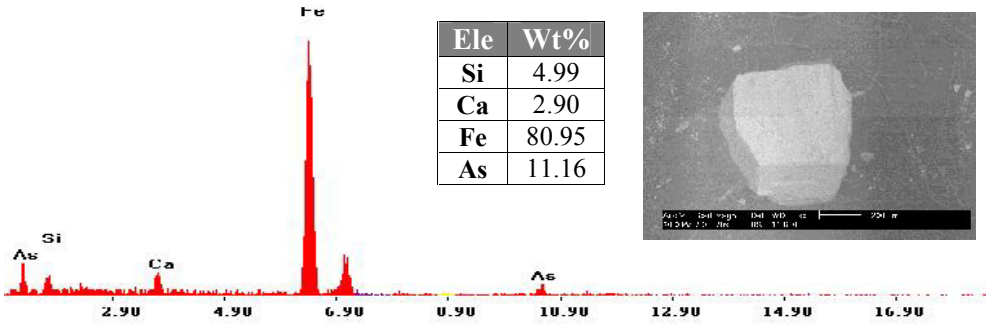


Fig.26: ESEM image and EDX analysis data of goethite

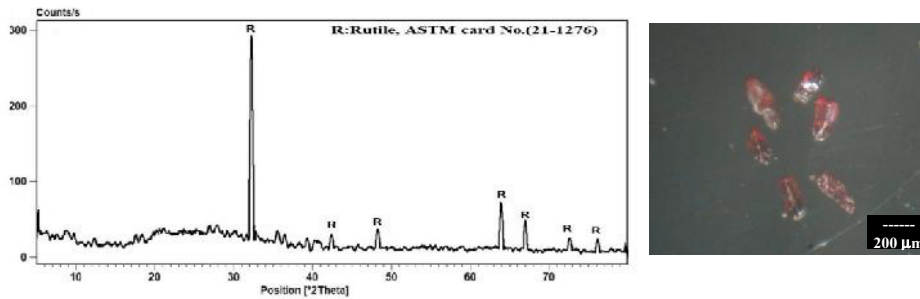


Fig.27: X-ray diffraction patterns of rutile

tile was analyzed by x-ray diffraction (Fig. 27) and ESEM technique (Fig. 28).

Pyrolusite (MnO_2), represents one of the most commonly manganese minerals, formed under highly oxidizing conditions in the oxidized zone of ore deposits. Mn-oxides may also be displayed as dendrites on fracture surfaces of rocks with grey or black color. EDAX analysis data show that pyrolusite have 71.73% Mn with minor Pb, Fe, K, Si, Al and Ca (Fig. 29).

Silicate Minerals

Kaolinite [$Al_2Si_2O_5(OH)_4$], is an import-

ant hydrothermal mineral and occurs abundantly in hydrothermal rocks. The process of hydrothermal alteration is responsible for its formation and weathering of intermediate basic and acidic rocks. It is appear as complex crystals associate with quartz grains (Fig.30). The XRD diffractogram (Fig.30) shows the presence of kaolinite associating quartz. EDX analyses show that kaolinite have 43.13% Al and 41.88% Si (Fig.31).

Spessartine [$Mn_3Al_2(SiO_4)_3$], represents one of the garnet groups which are closely related minerals. The color of garnets is extremely variable but is mainly controlled by the amount of Fe, Mn and Cr present (Deer et

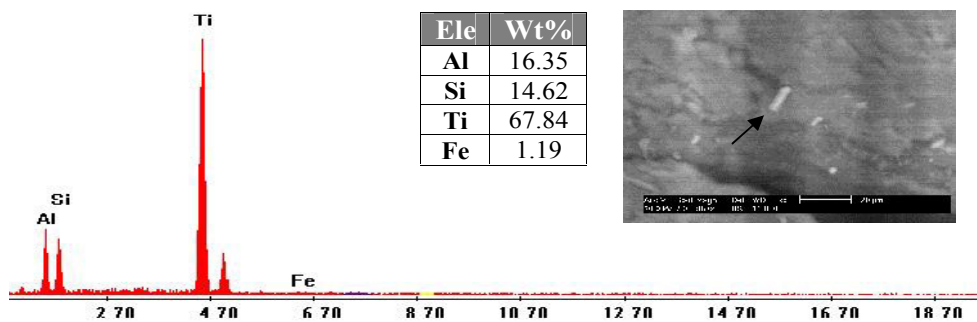


Fig.28: ESEM image and EDX analysis data of rutile

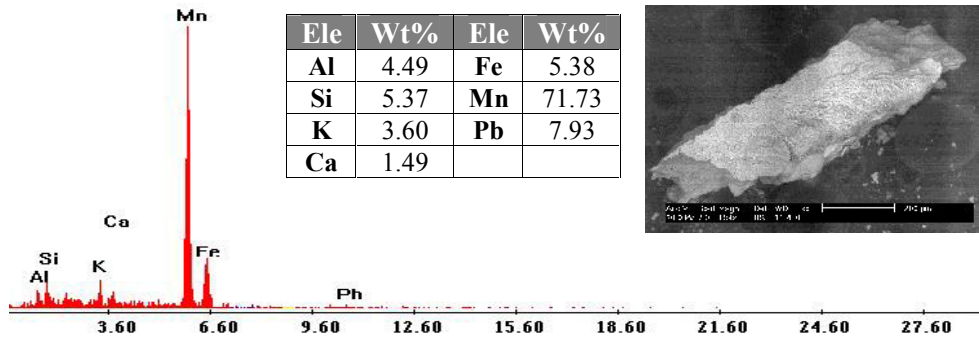


Fig.29: ESEM image and EDX analysis data of pyrolusite

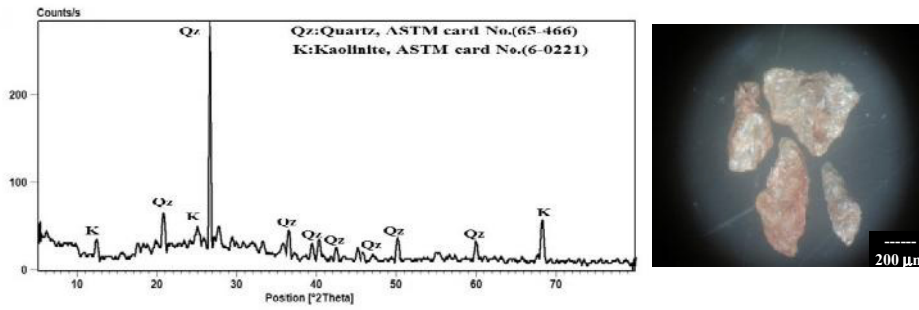


Fig.30 : X-ray diffraction patterns of kaolinite

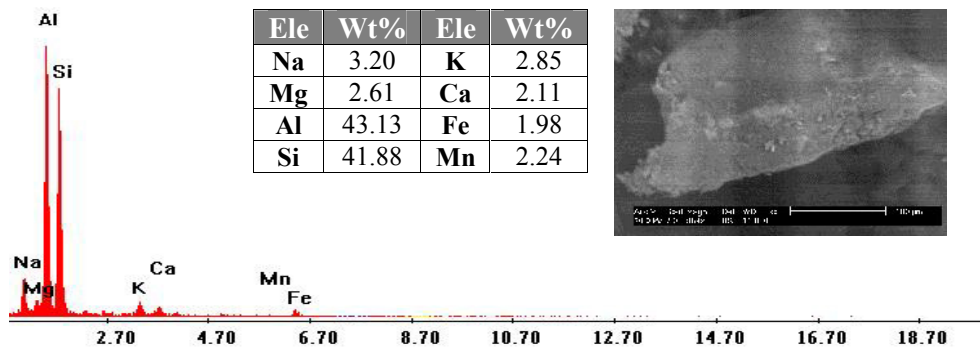


Fig.31: ESEM image and EDX analysis data of kaolinite

al., 1992). Spessartine mineral is represented by dark orange color (Fig.32), vitreous luster and white streak. The X-ray diffraction analysis recorded spessartine mineral (Figs. 32). Sub-angular to sub-rounded spessartine mineral 33.39% Al, 47.57% Si, 3.04% Mn by ESEM (Fig. 33).

GEOCHEMICAL AND RADIOMETRIC ANALYSIS

The quartz veins samples of Romit area were analyzed quantitatively for U, Th, major constituents and trace elements (Table 1).

The studied quartz veins are characterized by average silica content (86.68%) accompanied with very low Al₂O₃, MgO, CaO,

The spider-diagram (Fig. 34) of the trace elements contents of the studied quartz veins normalized to the primitive mantle data (McDonough and Sun 1995) display enrichment of Rb, U, Th, Zr, Nb, Pb and Y and depletion Ba and Sr. These enrichment and depletion of the compatible elements in the examined quartz veins are due to the effects of assimilation of crustal materials.

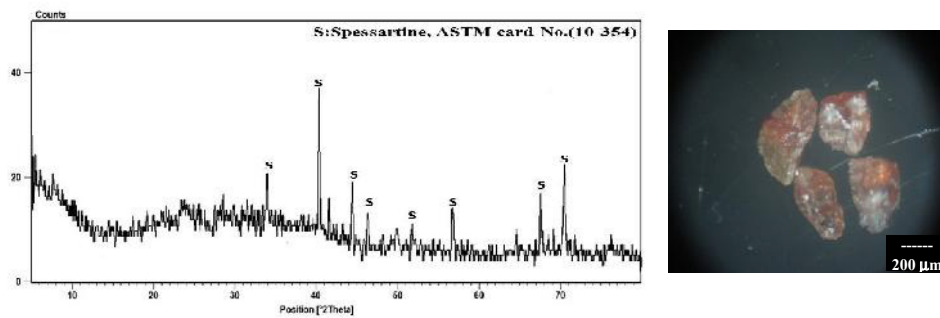


Fig.32: X-ray diffraction patterns of spessartine

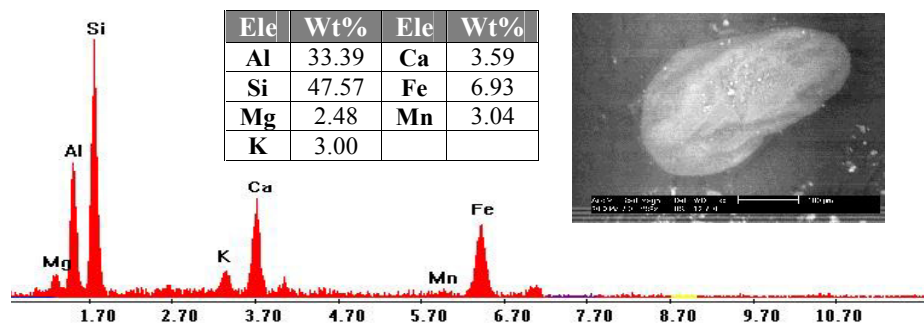


Fig.33: ESEM image and EDX analysis data of spessartine

Table 1: Chemical analyses of major oxides (wt%) and trace elements (ppm) for the quartz veins of Romit area

Elements	Quartz veins						Average
	R1	R2	R3	R4	R5	R6	
<i>Major oxides (wt. %)</i>							
SiO ₂	86.61	87.45	88.34	85.21	84.89	87.55	86.68
Al ₂ O ₃	2.23	1.6	2.67	2.67	1.86	1.79	2.14
TiO ₂	0.19	0.05	0.22	0.17	0.16	0.35	0.19
Fe ₂ O ₃	2.6	3.02	2.46	3.44	3.23	2.66	2.90
CaO	0.84	0.75	0.76	0.89	0.67	0.69	0.77
MgO	0.65	0.98	0.77	1.1	1.23	0.87	0.93
MnO	0.55	0.34	0.15	0.23	0.43	0.2	0.32
Na ₂ O	0.8	0.85	1.03	0.97	0.98	0.96	0.93
K ₂ O	0.9	0.98	1.32	1.17	1.54	0.89	1.13
P ₂ O ₅	0.27	0.16	0.12	0.09	0.11	0.07	0.14
LOI	2.98	2.48	1.65	2.57	3.33	3.2	2.70
Total	98.62	98.66	99.49	98.51	98.43	99.23	98.82
<i>Trace elements (ppm)</i>							
Cr	227	321	294	234	340	150	261
Ni	9	10	8	18	56	24	21
Cu	13	21	28	30	19	22	22
Zn	72	88	131	57	97	101	91
Zr	221	310	220	162	134	168	203
Ga	36	27	28	16	29	13	25
Sr	5	11	8	7	15	9	9
Y	281	298	342	272	249	289	289
Rb	2	8	9	15	20	12	11
V	2	5	4	3	8	5	5
Nb	40	41	23	16	56	34	35
Pb	1080	980	769	1100	963	789	947
Ba	47	46	57	78	81	56	61
Au	0.36	0.84	1.02	-	0.49	0.24	0.49
U	56	72	55	41	49	23	49
Th	73	89	98	63	77	50	75
Th/U	1.30	1.24	1.78	1.54	1.57	2.17	1.30

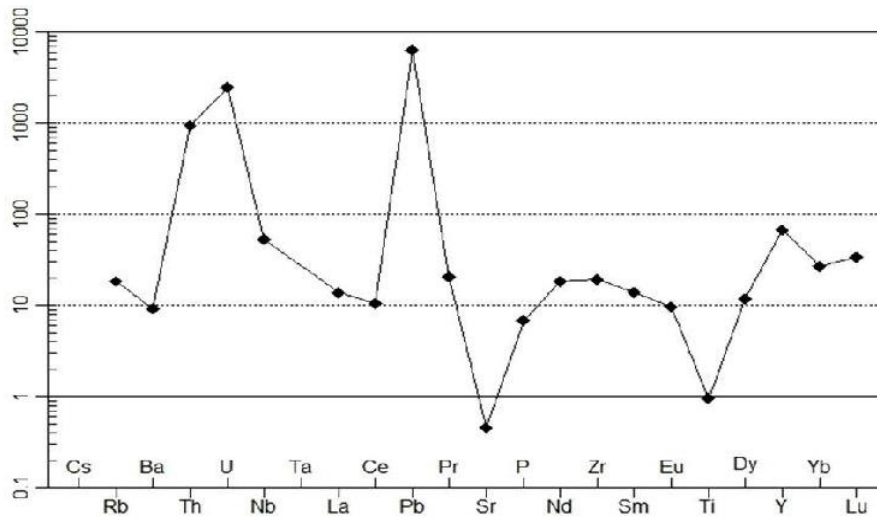


Fig. 34: Primitive-mantle normalized multi-element diagram (McDonough and Sun 1995) of the quartz veins of Romit area

RARE EARTH ELEMENTS

The mean abundances of rare earth elements, and the shape and slope of chondrite-normalized REE patterns, are distinctive for quartz samples. It is impossible for REE to act as isomorphism exit in quartz crystal because the ionic radius of most of REE is far longer than that of Si (Mu, 1999). The REE in quartz are mainly concentrated in fluid inclusion. The REE in fluid had not been impacted by quartz crystal that cannot be shaped by REE in its hydrothermal metasomatism and precipitation process. REE of quartz which are analyzed represent the REE in hydrothermal fluid. As a good geochemical tracer, changes in REE characteristics are often interpreted as changes in the source of fluid (Li et al., 2003).

Generally, the rock is characterized by relatively high content of rare earth elements with average 114.51 ppm that are attributed to the presence of the REE-bearing accessory

minerals as proved by EDX analyses as monazite, allanite and xenotime minerals. The chondrite-normalized REEs pattern (Boynton, 1984) is characterized by negative Eu and Ce anomalies (Fig. 35) with enrichment trend from LREEs (61.45 ppm) to HREEs (53.06 ppm), (Table2).

Eu as an oxidation sensitive element among REE, and is strongly dependent on temperature of depositional conditions (Dill, 2016, 2017). In fact, at temperatures $> 200^{\circ}\text{C}$ Eu^{3+} is reduced to mobile Eu^{2+} . Therefore, reduced Eu (Eu^{2+}) preferentially remains in solutions and causes negative anomaly in chemical/biochemical precipitates. In contrast, in low-temperature environments the immobile Eu^{3+} prevails and concentrates in chemical/biochemical carbonate precipitates, hence displaying positive Eu anomalies. The studied samples have negative Eu anomaly, reflecting reducing conditions in the depositional environment.

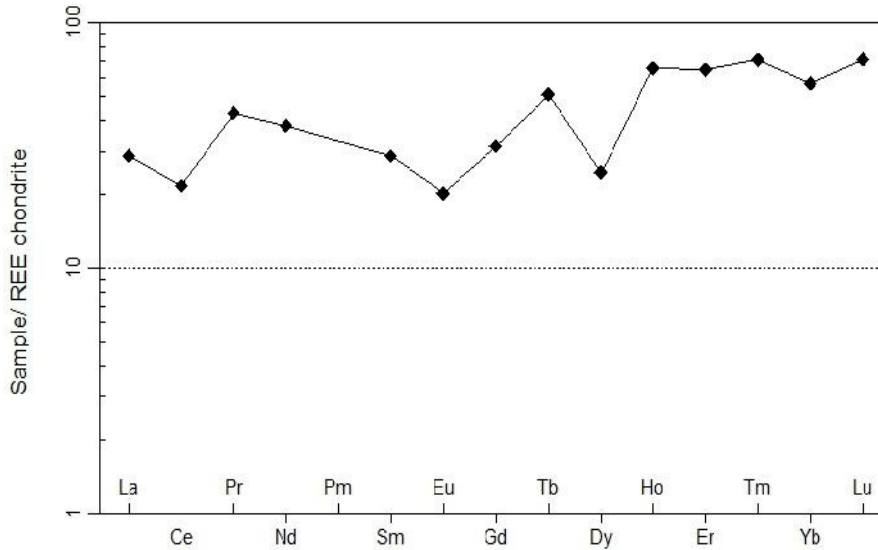


Fig. 35: Chondrite-normalized REE's (Boynton, 1984) of the quartz veins.

Under the condition of higher oxygen fugacity, Ce^{3+} can oxidize more easily to Ce^{4+} valence, which tends to remain in hydrothermal fluid resulting in positive Ce anomaly. Therefore, quartz with negative Ce anomaly and its being weak or strong are related to redox conditions of the fluid of quartz crystallization (Li et al., 2003; Mu, 1999). The oxygen fugacity was recorded in the quartz samples in their growth environment by negative Ce anomaly. Ce/Ce^* and Eu/Eu^* minimum in quartz samples which indicates that gold was precipitated in the sudden transformation from strong oxidized conditions to reduced conditions (Li et al., 1996).

Kawabe (1995) stated that the 'tetrad effect', 'double-double effect', or 'zigzag effect' are a characteristic feature of REE normalized patterns and could be used to exhibit the geochemical processes. The quantification of the tetrad effects shows the presence of M-type (convex) first tetrad (T1) in sample R6 while W-type (concave) in the

third and fourth tetrad (T3 and T4) in the rest samples (Table2). Unusual M- and W-type shape in the normalized REE pattern may clarify the role of hydrothermal alteration, in addition to water-rich solutions in the radioactive and gold mineralization (Abedini et al. 2018; Abed et al. 2022). This may be related to drastic changes in physico-chemical conditions at these rocks.

The ratio La_N/Yb_N is considered by Rollinson (1994) as a measure of the degree of fractionation of REEs in the melt. Calculation of this ratio for the rock under consideration showed that the REEs are fractionated with low degrees (average 0.50, Table2) indicating that they are slightly fractionated in the melt and highly fractionated in the accessory minerals. Plotting of the same ratio versus Ce_N showed positive relation referring to increasing of the degree of fractionation with increasing of the LREE represented by Ce (Fig.36).

Plotting of Th versus Ce/Th ratio (Fig.37) and U versus Ce/U (Fig.38) exhibit negative

Table 2: Chemical analyses of rare earth elements (ppm) for the quartz vein of Romit area

Elements	Quartz veins						Average
	R1	R2	R3	R4	R5	R6	
La	7.56	5.06	12.1	8.64	9.77	10.23	8.89
Ce	15.1	13.23	20.35	17.73	19.05	19.33	17.47
Pr	4.66	3.57	6.21	5.29	5.77	5.86	5.23
Nd	21	18.01	26.64	21.85	24.55	24.7	22.79
Sm	4.8	3.65	7.64	5.22	6.12	6.1	5.59
Eu	1.05	0.87	2.05	1.44	1.57	1.91	1.48
Gd	6.34	5.87	9.5	9.35	8.47	9.39	8.15
Tb	1.09	0.98	3.52	2.67	3.2	3.07	2.42
Dy	7.87	5.13	9.13	7.43	8.88	8.9	7.89
Ho	4.13	3.11	5.55	4.76	5.17	5.33	4.68
Er	11.25	10.45	17.42	12.44	14.16	15.24	13.49
Tm	2.02	1.79	2.75	2.29	2.31	2.56	2.29
Yb	10.35	9.07	16.34	10.75	10.8	13.83	11.86
Lu	1.86	1.55	2.9	2.01	2.56	2.83	2.29
Σ REEs	99.08	82.34	142.1	111.87	122.38	129.28	114.51
Σ LREEs	54.17	44.39	74.99	60.17	66.83	68.13	61.45
Σ HREEs	44.91	37.95	67.11	51.7	55.55	61.15	53.06
Eu/Eu*	0.58	0.57	0.74	0.63	0.67	0.77	0.66
Ce/Ce*	0.68	0.82	0.62	0.72	0.69	0.67	0.70
La _N /Yb	0.49	0.38	0.50	0.54	0.61	0.50	0.50
N							
t ₁	0.94	1.02	0.88	0.99	0.96	1.66	1.08
t ₃	0.62	0.57	0.85	0.73	0.88	0.80	0.74
t ₄	1.04	1.04	0.98	1.03	0.86	0.82	0.96
TE _{1,3}	0.77	0.76	0.87	0.85	0.92	0.87	0.84
TE _{1,4}	0.99	1.03	0.93	1.01	0.91	1.17	1.01

relations indicating that the radioelements are not hosted only in the accessory minerals but tend to form their own minerals.

The U and Th contents have average of 49 ppm and 75 ppm, respectively (Table 1). The concentrations of U and Th in the individual mineralized samples are primarily depending on the abundances of U- and Th-bearing minerals such as kasolite and uranothorite. The strong positive correlation between U and Th (Fig. 39), indicated that these two elements are connected together in the mineralization

processes and mainly incorporated in uranothorite.

The variation between U with Th/U ratios shows negative correlation (Fig. 40 and 41) this suggests that the distribution of radioactive elements is not only magmatic but also due to hydrothermal activity. Also, the Th/U value of the studied rocks reflects the oxidation-reduction features of the geological environment (Jones and Manning, 1994): (1) the Th/U value of the oxidizing environment is less than 0.75; (2) Th/U=0.75-1.25 represents

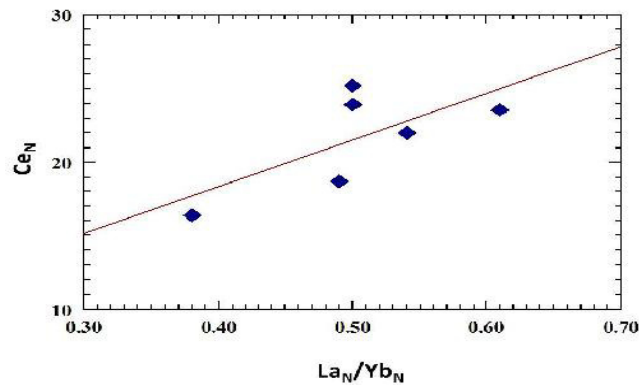


Fig.36: Degree of fractionation vs Ce_N of the quartz veins

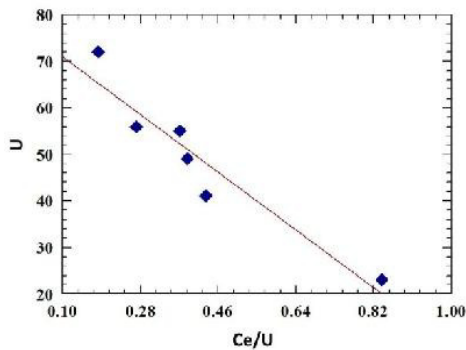


Fig. 37: U-Ce/U ratio of the quartz veins

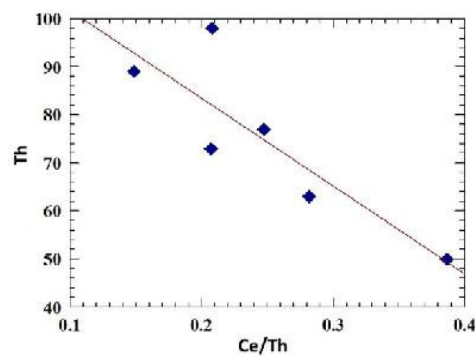


Fig.38: Th-Ce/Th ratio of the quartz veins

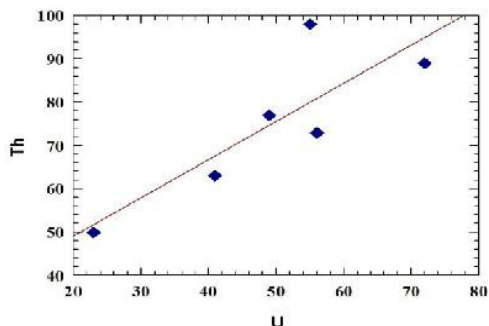


Fig. 39 : U-Th ratio of the quartz veins

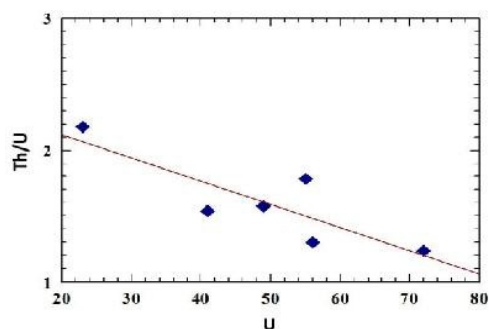


Fig.40: U-Th/U ratio of the quartz veins

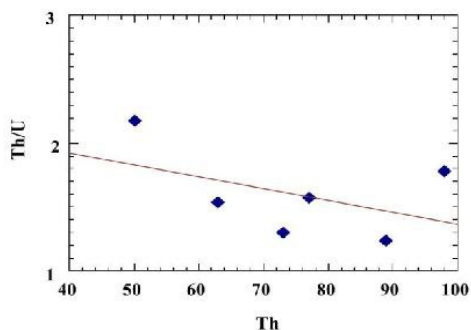


Fig. 41: Th-Th/U ratios of the quartz veins

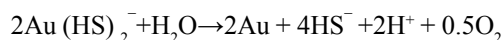
a transitive anoxic environment; (3) the value of Th/U of the reductive environment is greater than 1.25. The average value of Th/U is 1.30 displays the reducibility of the ore-forming fluids.

On the light of the presence of gold detected during the mineralogical and SEM techniques in quartz veins samples. This result led to analysis of bulk samples of them using fire assay technique at the Central Laboratories of the Egyptian Mineral Resources Authority (EMRA). The gold content ranges between 0.24 and 1.02 ppm with an average of 0.49 (Table 1).

THE GENESIS OF MINERALIZATION

The mineralogical studies confirm the presence of two mineralization stages, the earliest mineralization stage (high temperature stage) which is characterized by the formation of native Au associated with primary sulfide minerals such as pyrite and arsenopyrite. The high temperature stage was followed by a second lower-temperature stage characterized by the formation of secondary minerals; goethite and kaolinite.

The recorded gold contents in Romit area, considered as first record. The quartz veins samples have higher content of gold (ranges from 0.24 to 1.02 g/t). The occurrence of gold mainly depends on temperature, pressure, pH values, Cl^- concentration and fugacity of H_2S in a hydrothermal system. Gold mostly occurs as $AuCl_2$ in a system with temperature higher than $400^\circ C$ (Gammons and Williams-Jones, 1997), and with decreasing temperature being the primary mechanism causing gold deposition. $Au(HS)_2^-$ is the dominant phase at lower temperature with the decline of oxygen fugacity, the Au-S complex breaks down, leading to gold precipitation (Cooke and Simmons, 2000; Robb, 2005):-



The rare metals enrichment in the study area are formed due to the subsequent processes; including the ascending hydrothermal solution, with further contribution of the descending acidic meteoric water; supergene enrichment processes. The alkaline hydrothermal solution in quartz veins was under pH more than 7 and T. (300°C to 350°C). The acidic solution was under pH ranges from 2 to 3 with low temperature varying between 200°C to 250°C (Helgeson, 1969).

Precipitation of goethite is due to extensive alteration of pyrite and probably decreased the pH of the alkaline solution and rising acidic fluids. The presence of clay minerals indicates a high temperature environment (higher than 200°C). The mixing of volatile fluids with meteoric water and fluid-wall rock interaction result in changes in pH and oxygen activity and deposition of hypogene rare metals (gold) and supergene ones (goethite, kaolinite and secondary uranium) filling fractures.

The sudden change in the pH and temperature of the fluids will lead to destabilization of rare metal complexes favoring their deposition (Alexandrov et al., 1985). The rare metals mineralization are accumulate in the residual melt of the late fractionate (Bright, 1974) especially upward in the magmatic system (Smith, 1979).

Depending on Oxygen fugacity (fO_2) in the final magmatic fractionation, uranium tend to form the relatively soluble uranyl ion (UO_2^{+2}), hence, hydrothermal processes during final stages of crystallization of magma are important in controlling the later redistribution of uranium within the rocks (O'Connor et al., 1982). The origin of uranium appears to be closely associated with the rare metals mineralization and may be reflects readily their intimate coherence.

REE mobility is favored by: low pH, high water rock ratios and abundant complexing ions (CO_3^{2-} , F^- , Cl^- , PO_4^{3-} , and SO_4^{2-}) in the hydrothermal solutions (Michard, 1989 and Lottermoser, 1992).

The REE in Romit quartz veins were brought by hydrothermal fluids into rocks during alteration and may be precipitated such as monazite and allanite.

CONCLUSIONS

Romit area lies at Gabal Ti Keferiai which is located in the southern extremity of the Eastern Desert of Egypt near the Sudan frontier between Latitudes 22° 14' 29" and 22° 28' 25" N and Longitudes 35° 34' 21" and 36° 01' 09" E. Metavolcanics and tonalite-granodiorites form most of the outcrops in the area which are cutting by Quartz veins.

The quartz veins have a strong enrichment in some rare metal (which Zr, Y, Nb, Pb and Au). Quartz veins show an average result of fire assay of gold is 0.49 ppm. Chondrite normalized REE diagram shows that the quartz veins have enrichment of Σ REE with low degree of fractionation in the melt (0.50) and in turn, high degree of fractionation in the accessory minerals and displays progressive enrichment in LREE relative to HREE. The enrichment of REE may be attributed to the presence of monazite and allanite as a source of LREE and xenotime and garnet as a source for HREE.

The quartz veins show slightly high level of radioactivity giving U average content of 49 ppm while, Th average content is 75 ppm. The present study proved that radioactive minerals responsible for U and Th in the studied quartz veins are kasolite and uranothorite. The Th/U values reflect the reducibility of the ore-forming fluids, coincident with the sulphide minerals (pyrite, arsenopyrite) which indication of gold.

It may be concluded that the hydrothermal fluids responsible for the formation of the studied silica veins and the deposition of Au and U mineralizations in these veins, suffered different physico-chemical changes allowing transportation and the associated deposition of Au and U together with sulphides in the study silica veins.

Acknowledgements

I am indebted to Prof. Mohamed G. El-Feky of NMA for great helpful and reviewing the manuscript.

REFERENCES

- Abed, N. S.; El Feky, M.G.; El-Taher, A.; Massoud, E. E.; Khattab, M. R.; Alqahtani, M. S.; Yousef, E., and Hanfi, M.Y., 2022. Geochemical Conditions and Factors Controlling the Distribution of Major, Trace, and Rare Elements in Sul Hamed Granitic Rocks, Southeastern Desert, Egypt. *Minerals*, 12, 1245. <https://doi.org/10.3390/min12101245>.
- Abedini, A.; Azizi, M. R., and Calagar, A. A., 2018. The Lanthanide Tetrad Effect in Argillic Alteration: An Example from the Jizvan District, Northern Iran. *Acta Geologica Sinica*, 92, 4, 1468–1485.
- Alexandrov, I.V.; Krasov, A.M., and Kochnova, L.N., 1985. The effects of K, Na and F on rock-forming mineral assemblages and the formation of tantalum-niobate mineralization in rare-element granite pegmatites. *Geochem. Inter.*, 22, 85-92.
- Ammar, S.E., 1997. Uranium and thorium mineralization at northern part of Gabal Um Naggat stock, Central Eastern Desert. Egypt. *Mans. Sci. Bull.* 24 (2), 11–44.
- Ammar, F.; Omar, S., and El Sawey, E.S., 2016. Genetic affiliation of gold and uranium mineralization in El-Missikat granite, Central Eastern Desert, Egypt. *NSSJ* 5, 33–47.
- Assaf, H.S.; Ibrahim, M.E.; Ammar, S.E.; Saleh, G.M., and Hashed, M.A., 1998. Geological and mineralogical studies on the radioactive mineral occurrence at Qash Amir area, South Eastern Desert, Egypt. Inter. report, NMA, Cairo, Egypt.
- Bassiuny, F.A., 1957. Mineral prospecting in Elba area during seasons 1956–1957, (Inter. report), Geol. Surv. Egypt, Cairo, Egypt.
- Basta, E.Z., and Saleeb, W.S., 1971. Mineralogy of the manganese ores of Elba area south Eastern Desert, U.A.R.. *J. Geol.*, 15 (1), 29–48.
- Boynton, W. V., 1984. Geochemistry of rare earth elements: Meteorite studies. In: Henderson, P., Ed., of rare earth elements geochemistry, Elsevier, New York, 63-114.
- Bright, M.J., 1974. Primary geochemical dispersion associated with the Henderson molybdenum deposit, Colorado. *Abst., Econ. Geol.*, 69, 1177.
- Burley, S.D.; Mullis, J.T., and Matter, A., 1989. Timing diagenesis in the Tartan Reservoir (UK North Sea): Constraints from combined cathodoluminescence microscopy and fluid inclusion studies. *Mar. Pet. Geol.*, 6, 98–120.
- Cooke, D.R., and Simmons, S.F., 2000. Characteristics and genesis of epithermal gold deposits. *Reviews in Economic Geology*. 13, 221e244.
- Dardir, A.A.; Naim, G.M.; Abdel-Kader, A.; Hussein, A.K.; Mansour A.M.; Gad, N.L., and Amin, H.M., 1992. Mineral resources of the Red Sea Governorate, development possibilities, Geol. Surv. Egypt, Cairo, Egypt.
- Deer, W. A.; Howie, R. A., and Zussman, J., 1992. An introduction to the rock forming minerals. Longman Group Limited, London, England. 2nd Ed., 696p.
- Dill, H.G., 2016. Kaolin: soil, rock and ore from the mineral to the magmatic, sedimentary, and metamorphic environments. *Earth Sci. Rev.*, 161, 16 –129. DOI: 10.1016/j.earscirev.2016.07.003.
- Dill, H.G., 2017. Residual clay deposits on basement rocks: The impact of climate and the geological setting on supergene argillitization in the Bohemian Massif (Central Europe) and across the globe. *Earth Sci. Rev.*, 165, 1–58. DOI: 10.1016/j.earscirev.2016.12.004.
- El Aify, Z.; Bagddady, M.; Awaga, G.; Morsei, A.; Ramadan, T.M., and Abdallah, M.A., 1994. Geochemical exploration of Elba-Gerf area,

- South Eastern Desert, (Inter. report) ,Geol. Surv. Egypt, Cairo, Egypt.
- El Gammal, E., and Cherif, O., 1999. Granitoid series and tungsten deposits in the Eastern Desert of Egypt. 12th symp. Precambrian and Development, Cairo, Egypt.
- El Ghawaby, M.A., 1973. Structures and radioactive mineralization of Wadi Zeidun area, Eastern Desert, Egypt. Ph. D. Thesis, Ain Shams Univ., Cairo, Egypt.
- El Kassas, I.A., 1974. Radioactivity and geology of Wadi Atalla area. Eastern Desert of Egypt, Arab Republic of Egypt. Ph. D. Thesis, Fac. Sci. Ain Shams Univ, Cairo, Egypt, 502p.
- El-Ramly, M.F., 1972. A new geological map for the basement rocks in the Eastern and Southwestern Desert of Egypt, Scale 1:1000,000. Ann. Geol. Surv. Egypt., II, 1-18.
- El-Shazly, E.M., and El Ghawaby, M.A., 1974. Tectonic analysis of Wadi Zeidun area and its application in localizing radioactive mineralization in the Central Eastern Desert, Egypt. 2nd Arb. Conf. Miner. Resour., Jeddah, Saudi Arabia. 20-43.
- El-Shazly, E.M., and Saleeb, G.S., 1959. Contribution to the mineralogy of Egyptian manganese deposits. Econ. Geol., 54 (5), 873-888.
- Gammons, C.H.; Yu, Y.M., and Williams Jones, A.E., 1997. The disproportionation of gold (I) chloride complexes at 25 to 200 °C. Geochim. Cosmochim. Acta ,61, 1971-1983.
- Götze, J., 2012. Classification, mineralogy and industrial potential of SiO₂ minerals and rocks. In Quartz: Deposits, Mineralogy and Analytics; Springer: Berlin/Heidelberg, Germany, 1-27.
- Helgeson, H.C., 1969. Thermodynamics of hydrothermal systems at elevated temperatures and pressures. Am. J. Sci., 267, 729-804.
- Hume, W.F., 1937. Geology of Egypt. Vol. II. The fundamental Precambrian rocks of Egypt and Sudan, Part I, The metamorphic rocks: 1-300, Part II, The later plutonic and minor intrusive rocks. Survey Dept., Cairo, Egypt, 301-688.
- Hussein, I.M., 1977. Geology of the Halaib area of the northern Red Sea Hills, Sudan, with reference to the Sol Flamed basic complex M. Sc.. Portsmouth Polytechnic, England.
- Hussein, A.A., 1990. Mineral deposits. In: Said, R. (Ed.), Geol. Egypt. Balkema, Rutterdam, p. 734.
- Basta, E.Z., Saleeb, W.S., 1971. Mineralogy of the manganese ores of Elba area south Eastern Desert, U.A.R.. J. Geol. 15 (1), 29-48.
- Jones, B.J., and Manning, A.C., 1994. Comparison of geochemical indices used for the interpretation of palaeoredox conditions in ancient mud stones (J). Chem. Geol. ,111, 111-129.
- Kabesh, M.I., 1994. A preliminary note on some granitoids, Halaib- Elba area. South Eastern Desert, Egypt. Egypt. Mineral., 6, 119-139.
- Kawabe, I., 1995. Tetrad effects and fine structures of REE abundance patterns of granitic and rhyolitic rocks: ICPAES determinations of REE and Y in eight GSJ reference rocks. Geochim. J., 29, 213-230.
- Kerr, P.F., 1959. Optical mineralogy. 3rd Ed., McGraw- Hill Book Company, Inc., New York, Toronto, London.
- Lazareva, E.V.; Zhmodik, S.M.; Prokopiev, A.V.; Karmanov, N.S., and Sergeenko, A.I., 2018. Nodular monazite from placers in the Kular Ridge (Arctic Siberia, Russia): Composition and age. Russian Geol. and Geophy., 59(10), 1330-1347. doi:10.1016/j.rgg.2018.09.010.
- Li, H. M.; Shen Y. C.; Mao J. W.; Liu T. B., and Zhu H. P., 2003. REE features of quartz and pyrite and their fluid inclusion: an example of Jiaojia-type gold deposits, northwestern Jiaodong peninsula. Acta Petrol Sin, 19 (2), 267-274 (in Chinese).

- Li, S. R.; Chen G. Y.; Shao W., and Sun D. S., 1996. Genetic mineralogy of Rushan gold deposit in Jiaodong peninsula. Beijing: Geological Publishing House (in Chinese).
- Lottermoser, B.G., 1992. Rare earth elements and hydrothermal ore formation processes. *Ore Geol. Rev.*, 7, 25-41.
- McDonough, W. F., and Sun, S., 1995. The composition of the Earth, *Chem. Geol.*, 120, 223-253.
- Michard, A., 1989. Rare-earth element systematics in hydrothermal fluids. *Geochim. Cosmochim. Acta*, 53, 745-750.
- Mu, B. L., 1999. *Element Geochemistry*. Beijing: Peking University Press (in Chinese).
- O'Connor, P. J.; Hennessy, J.; Bruch, P. M., and Williams, C. T., 1982. Abundance and distribution of uranium and thorium in the northern units of the Leinster granite, Ireland. *Geol. Mag.*, 119 (6), 581 - 592.
- Pirajno, F., 2009. *Hydrothermal Processes and Mineral Systems*. Springer Science & Business Media: Berlin, Germany.
- Ramadan, T.M., 2003. Use of ERS-2 SAR and Landsat TM Images for Geological Mapping and Mineral Exploration of Sol Hamid Area, South Eastern Desert, Egypt. *Egypt. J. Remote Sensing Space Sci.*, 5, 13-24.
- Ramadan, T.M., and Sultan, A.S., 2004. Integration of remote sensing and geophysical data for the identification of massive sulphide zones at Wadi Allaqi area, South Eastern Desert, Egypt. M.E.R.C. Ain Shams Univ., Earth Sci. Ser. 18, 165-174.
- Robb, L., 2005. *Introduction to Ore-forming Processes*. Blackwell Publishing, Malden, 373 pp.
- Rollinson, H.R., 1994. *Using geochemical data: evaluation, presentation, and interpretation*, Longman Scientific & Technical, Singapore. 352p.
- Rusk, B., 2012. Cathodoluminescent textures and trace elements in hydrothermal quartz. In *Quartz: Deposits, Mineralogy and Analytics*; Springer: Berlin/Heidelberg, Germany, 307-329.
- Shahin, H.A.A., and Masoud S. M., 2014. Hydrothermally altered and fractured granite hosting rare metal at Gabal Adara Adatalob, South Eastern Desert, Egypt. *Earth sciences.*, 3, No. 1, 1-7. Doi:10.11648/j.earth.s.20140301.11.
- Shapiro, L., and Brannock, W.W., 1962. Rapid analysis of silicate, and carbonate phosphate rocks, *U.S. Geol. Surv. Bull*, 114A, 56p.
- Smith, R.L., 1979. Ash-flow magmatism. *Geol. Soc. Amer. Spec. Paper* 180, 5-27.
- Takla, M.A.; Basta, E.Z.; El-Sharkawi, M.A., and Fawzie, E., 1976. The Mineralogy of some wolframite veins from Egypt. *Bull. Fac. Sci., Cairo, Univ.*, 49.
- Takla, M.A., and Hussein, A.A., 1995. Shield rocks and related mineralizations in Egypt. 11th *Sympos. Precamb. Dev., Cairo, Abst.*, 6-7.
- Zeid, E.K.A., 2020. Autunite-group minerals their paragenesis from the sheared granite of Gabal El Sela, South Eastern Desert, Egypt. *Open J. Geol.*, 10, 703-725.
-

جيولوجية و جيوكيميائية عروق الكوارتز الحاو لمعدن الذهب بمنطقة روميت, جنوب الصحراء الشرقية - مصر

مصطفى بيومي مصطفى و دعاء انور مصطفى

تقع منطقة روميت في الجزء الجنوبي من الصحراء الشرقية بالقرب من حدود السودان وتغطي المنطقة بالصخور النارية و المتحولة حيث تكون صخور البركانيات المتحولة وصخور التوناليت -جرانوديوريت معظم مكاشف المنطقة. منطقة الدراسة منقطعة بعدد كبير من عروق الكوارتز التي تحوى معادن اليورانيوم و الثوريوم و المعادن الارضية النادرة والذهب.

أمكن تقسيم المعادن الثقيلة المحتواه الى أربع مجموعات هي مجموعة المعادن الحاملة لعناصر اليورانيوم والثوريوم والعناصر الأرضية النادرة (الكازوليت-اليورانوثوريت-الكولمبيت-المونازيت-الألنيت-الزيتونيم)، مجموعة معادن الفلزات القاعدية (الذهب-البيريت-الارزنيوبيريت-سيروسيت)، مجموعة معادن الأوكسيد (الكروميت-الجوثيت-الروتيل-البيرولسيت) ومجموعة السيلكات (الكاولينيت-سبيسرئين).

توضح نتائج التحاليل الكيميائية إن عروق الكوارتز من الممكن أن تحوي أو تعمل كمصدر لتمعدنات الفلزات النادرة (الزركونيوم والإتريوم والرصاص والنيوبيوم والذهب) وهذا يعزي الى تأثير المحاليل الحارمانية في المراحل المتأخره من النشاط الجماتي.

أوضحت دراسة العناصر الارضية النادرة لعروق الكوارتز باستخدام علاقه الكوندرت وجود قيمة سالبة لشادات الاروبيوم والسيريوم أن هناك اثرء للعناصر الارضية النادرة الخفيفة مقارنة بنظيراتها الثقيلة وهذا ما تؤكدته الدراسات المعدنية والتي تظهر تواجد معادن المونازيت والالانيت كمصدر للعناصر الارضية النادرة الخفيفة بينما يمثل تواجد معادن الزيتونيم والجارنت مصدر للعناصر الارضية النادرة الثقيلة.

أوضحت الدراسة الاشعاعيه لصخور عروق الكوارتز ان متوسط اليورانيوم ٤٩ جزء في المليون والثوريوم ٧٥ جزء في المليون وأرجعت ذلك الى تواجد معادن الكازوليت واليورانوثيريت.